Gene therapy of metachromatic leukodystrophy reverses neurological damage and deficits in mice

Alessandra Biffi, … , Angelo Quattrini, Luigi Naldini

Research Article   **Genetics**

Metachromatic leukodystrophy (MLD) is a demyelinating lysosomal storage disorder for which new treatments are urgently needed. We previously showed that transplantation of gene-corrected hematopoietic stem progenitor cells (HSPCs) in presymptomatic myeloablated MLD mice prevented disease manifestations. Here we show that HSC gene therapy can reverse neurological deficits and neuropathological damage in affected mice, thus correcting an overt neurological disease. The efficacy of gene therapy was dependent on and proportional to arylsulfatase A (ARSA) overexpression in the microglia progeny of transplanted HSPCs. We demonstrate a widespread enzyme distribution from these cells through the CNS and a robust cross-correction of neurons and glia in vivo. Conversely, a peripheral source of enzyme, established by transplanting ARSA-overexpressing hepatocytes from transgenic donors, failed to effectively deliver the enzyme to the CNS. These results indicate that the recruitment of gene-modified, enzyme-overexpressing microglia makes the enzyme bioavailable to the brain and makes therapeutic efficacy and disease correction attainable. Overall, our data provide a strong rationale for implementing HSPC gene therapy in MLD patients.

Find the latest version:

https://jci.me/28873/pdf

Gene therapy of metachromatic leukodystrophy reverses neurological damage and deficits in mice

Alessandra Biffi,[1,2] Alessia Capotondo,[1,2] Stefania Fasano,[3] Ubaldo del Carro,[4] Sergio Marchesini,[5] Hisaya Azuma,[6] Maria Chiara Malaguti,[4] Stefano Amadio,[4] Riccardo Brambilla,[3] Markus Grompe,[6] Claudio Bordignon,[1,2] Angelo Quattrini,[4] and Luigi Naldini[1,2]

[1]San Raffaele Telethon Institute for Gene Therapy, [2]Vita-Salute San Raffaele University, [3]Department of Molecular Biology and Functional Genomics, and [4]Neurology Unit, San Raffaele Scientific Institute, Milan, Italy. [5]Department of Biomedical Science and Biotechnology, University of Brescia, Brescia, Italy. [6]Department of Medical and Molecular Genetics, Oregon Health and Science University, Portland, Oregon, USA.

Metachromatic leukodystrophy (MLD) is a demyelinating lysosomal storage disorder for which new treatments are urgently needed. We previously showed that transplantation of gene-corrected hematopoietic stem progenitor cells (HSPCs) in presymptomatic myeloablated MLD mice prevented disease manifestations. Here we show that HSC gene therapy can reverse neurological deficits and neuropathological damage in affected mice, thus correcting an overt neurological disease. The efficacy of gene therapy was dependent on and proportional to arylsulfatase A (ARSA) overexpression in the microglia progeny of transplanted HSPCs. We demonstrate a widespread enzyme distribution from these cells through the CNS and a robust cross-correction of neurons and glia in vivo. Conversely, a peripheral source of enzyme, established by transplanting ARSA-overexpressing hepatocytes from transgenic donors, failed to effectively deliver the enzyme to the CNS. These results indicate that the recruitment of gene-modified, enzyme-overexpressing microglia makes the enzyme bioavailable to the brain and makes therapeutic efficacy and disease correction attainable. Overall, our data provide a strong rationale for implementing HSPC gene therapy in MLD patients.

Introduction

Metachromatic leukodystrophy (MLD) is an autosomal recessive lipidosis caused by the deficiency of the lysosomal enzyme arylsulfatase A (ARSA) and can be considered a lysosomal storage disorder (LSD) with predominant neurological involvement (1, 2). The enzymatic defect results in the accumulation of the ARSA substrate galactosylceramide I^3-sulfate (sulfatide), a major sphingolipid of myelin. The disease is characterized by myelin degeneration in both the CNS and peripheral nervous system (PNS), associated with the accumulation of sulfatide in glial cells and neurons. Despite the fact that the enzymatic deficiency is systemic, disease manifestations are restricted to the nervous system. Children affected by MLD display progressive neurologic symptoms, including ataxia, seizures, and quadriplegia, culminating in decerebration and eventual death early in infancy (1, 2).
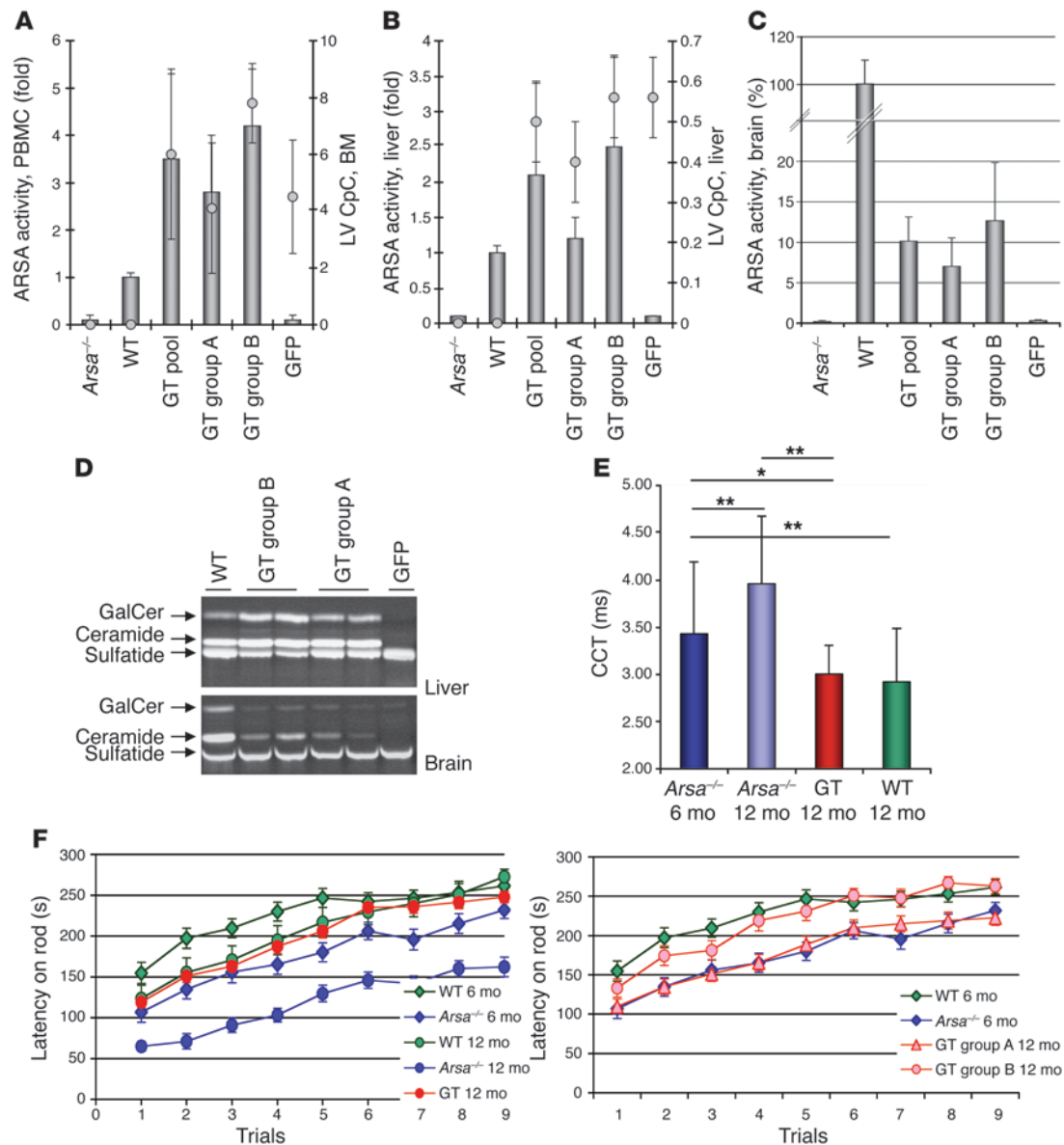
As is true for other LSDs affecting the CNS, there is currently no effective treatment for MLD, and the benefits of allogenic hematopoietic stem cell transplantation (HSCT) are still controversial

(3, 4). Allogenic HSCT corrects the metabolic deficiency in hematopoietic lineages. Furthermore, some of the progeny of engrafted hematopoietic stem progenitor cells (HSPCs) migrate extravascularly and release some functional enzyme in the affected tissues (5). As cells can take up extracellular enzyme by the mannose 6-phosphate (M6P) receptor and correct their defect in vitro (6, 7), it is thought that a similar process of cross-correction may occur in vivo. Several preclinical and clinical studies support the notion that enzymatic cross-correction of the liver and other visceral organs is substantial after HSCT or enzyme replacement therapy in LSDs (8). However, a similar bioavailability of functional enzyme in the CNS is more difficult to achieve. Consistent with this limitation, HSCT has generally had a poor outcome in neurodegenerative storage disorders. Recent clinical studies in globoid cell leukodystrophy report clinical benefits of transplanting BM (4) and umbilical cord blood (9) HSPCs if the procedure is performed soon after birth, at a presymptomatic stage. The same treatment was ineffectual when applied to symptomatic patients (9), suggesting either that recruitment of the HSPC progeny to the CNS is too slow to reverse the disease once it is established or that unique permissive conditions for CNS cross-correction are in place in the perinatal period. Besides its limited efficacy, allogenic HSCT is associated with substantial morbidity and mortality and may adversely affect disease outcome per se. Moreover, recent in vitro studies have raised the concern that macrophages and microglia, which are the HSPC progeny recruited to the CNS, may release lysosomal enzymes lacking the M6P recognition marker (10) and thus represent an inadequate source of enzyme for in vivo cross-correction. Regarding enzyme replacement therapy, studies conducted in murine models indicate that enzyme bioavailability is poor in the CNS when the blood-brain barrier (BBB) integrity is preserved, as is the case in MLD (11).

Figure 1
Enzymatic reconstitution and correction of neurological defects in *Arsa*^{-/-} mice. (**A**) ARSA activity in PBMC (left *y* axis) and LV content in BM (right *y* axis) of untreated (*Arsa*^{-/-}), mock-treated (GFP), and GT-treated (pool and groups A and B) *Arsa*^{-/-} mice and WT controls. ARSA activity is expressed as fold increase compared with WT levels and LV content in CpC. (**B**) ARSA activity (left *y* axis) and LV CpC (right *y* axis) from liver samples from the same groups as in **A**. (**C**) ARSA activity of brain extracts is expressed as percentage of WT values. For statistical analysis, see Table 1. (**D**) Representative TLC gel from Rh-sulfatide test on liver and brain extracts from the indicated mice groups. (**E**) Assessment of central motor conduction in untreated and mock-treated *Arsa*^{-/-} mice, 12-month-old GT mice (pool), and age-matched WT controls (*n* = 15 mice per group). The GT group showed significantly lower CCT as compared with 6-month-old and age-matched *Arsa*^{-/-} mice; comparison with WT mice showed normalization of CCT (*$P < 0.05$, **$P < 0.01$). (**F**) Behavioral evaluations of GT mice. Mean latencies on rotarod ± SEM for each day are indicated. The GT group was indistinguishable from age-matched WT controls (left panel). Twelve-month-old GT mice in group B had a significantly improved performance compared with 6-month-old *Arsa*^{-/-} mice, demonstrating correction of the neurological deficit present at the time of treatment (right panel). For statistical analysis, see Table 3 (*n* = 15–30 mice per group.). GalCer, galactosylceramide.

Thus, several biological and clinical factors severely limit the therapeutic potential of HSCT and enzyme replacement therapy for CNS storage disorders, and the development of new effective strategies is badly needed.

We and others have proved that HSCT combined with gene therapy (GT) may represent one such candidate strategy, as it combines advantages of an autologous HSPC source with the benefits of enzyme overexpression in transplanted cells (12–18). We recently demonstrated progressive and extensive reconstitution of well-differentiated microglia in the CNS by the transgene-expressing progeny of transplanted HSPCs in *Arsa*^{-/-} mice (14). Taking advantage of lentiviral vectors (LVs) to achieve efficient gene transfer into

Table 1
Dose-effect relationships in treated *Arsa*−/− mice

Treatments	n	CpC	ARSA activity			Neurophysiology		Hippocampus		Cerebellum	
			PBMC (fold to WT)	Liver (fold to WT)	Brain (% of WT)	CCT (ms)	Rotorod Latency (s)	Deposits, fimbria (score)	Neu damage, CA2–3 (% deg neu)	Deposits, white matter (score)	Neu damage, Purkinje (% deg neu)
UT *Arsa*−/−, 6 mo	36	–	0.3 ± 0.3	0.1	0.1	3.4 ± 0.7[A]	232 ± 10[B]	1.5 ± 0.5	17 ± 2.8	1.7 ± 0.5	41 ± 18
MT *Arsa*−/−, 12 mo	45	4.5 ± 2	0.3 ± 0.2	0.1	0.1	3.9 ± 0.7[B,C]	162 ± 12[B,D]	2.7 ± 0.6[D]	57 ± 9.8[D]	2.9 ± 0.7[D]	62 ± 20[C]
GT, pool, 12 mo	61	6 ± 3	3.5 ± 1.0[E]	2.1 ± 1[E]	10.1 ± 5.3[E]	3.0 ± 0.3[C,E]	248 ± 7[E]	1.5 ± 0.7[E]	26.5 ± 15[E]	1.8 ± 0.8[E]	32 ± 15[E]
GT, group A, 12 mo	36	4.1 ± 1.8	2.8 ± 0.8	1.2 ± 0.3	7 ± 2.5	3.2 ± 0.45[E]	223 ± 10[E]	1.8 ± 0.6[E]	40.9 ± 18	2.2 ± 0.7	45.5 ± 14
GT, group B, 12 mo	25	7.8 ± 1.4[F]	4.2 ± 1.0[F]	2.5 ± 0.9[F]	12.6 ± 4.2[E]	2.92 ± 0.1[C,E]	263 ± 10[D,E,F]	1.2 ± 1[E]	18.4 ± 7[E,F]	1.5 ± 0.8[E,F]	25.7 ± 8[D,E,F]
UT WT, 6 mo	29	–	1 ± 0.5	1 ± 0.3	100 ± 2.5	3.0 ± 0.4	262 ± 9	–	–	–	–
MT WT, 12 mo	20	5.1 ± 1.6	1 ± 0.5	1 ± 0.3	100 ± 2.5	2.9 ± 0.5	272 ± 9	–	–	–	–

We analyzed the following groups of mice: untreated (UT) or mock-treated (MT) *Arsa*−/− mice, the latter transplanted with *Arsa*−/− HSPCs transduced with GFP-LV; GT-treated mice (GT, pool and groups A and B; for details, see text); UT and MT WT animals at the indicated age in months. ARSA activity was quantified by p-NC assay on total PBMCs and by Rh-sulfatide test for liver and brain extracts and is expressed as fold increase compared with WT (fold to WT) or percentage (%) of WT levels. LV CpC was quantified by TaqMan on bone marrow DNA from transplanted mice. For rotarod test, the mean latency on rod measured at the ninth trial is reported. For histopathology, the semiquantitative score for white matter deposits and the percentage of degenerated neurons in hippocampal CA2–3 and Purkinje cell layer (neu damage) are reported. For statistical analysis, Student's t test and 2-way ANOVA were used for CpC, ARSA activity, and neurophysiology, and for behavior, respectively. [A]*P* < 0.05, [B]*P* < 0.01 for comparison with age matched WT groups; [C]*P* < 0.05; [D]*P* < 0.01 for comparison with 6-month-old UT *Arsa*−/−; [E]*P* < 0.01 for comparison with 12-month-old MT *Arsa*−/−; [F]*P* < 0.05 for comparison with group A.

HSPCs and long-term overexpression of the ARSA gene in their cellular progeny, we prevented the development of major disease manifestations in mice treated at the presymptomatic stage (14). Interestingly, transplantation of WT cells did not achieve significant clinical benefit, suggesting a critical role of enzyme overexpression in the success of our strategy.

Unfortunately, in most cases, and unless a family history is available, the diagnosis of MLD is made after the onset of symptoms. Thus, in order for a clinical benefit to be achieved in patients with an established neurologic disease, a new therapeutic strategy should be devised (19). Here we report complete normalization of established behavioral abnormalities, motor conduction deficits, and neuropathological alterations of *Arsa*−/− mice after HSPC GT. We demonstrate that microglia is the exclusive source of ARSA in the CNS and that enzyme transfer and robust cross-correction of neural cell targets occur in vivo. Thus, our results strongly support the use of HSPC GT in clinical trials for MLD patients.

Results

Correction of established neurological disease in GT-treated MLD mice. The mouse model of MLD, generated by targeted disruption of the murine ARSA gene *Arsa*, is characterized by slowly progressive CNS and PNS disease (20) and allows longitudinal evaluation of disease evolution. By 5–6 months of age, *Arsa*−/− mice already display motor coordination impairment, delayed motor conduction in the CNS and PNS, neuronal degeneration, and widespread storage of metachromatic material; further deterioration along these lines occurs with age (see below).

We transplanted HSPCs from *Arsa*−/− donors transduced with LV expressing either ARSA or GFP into a total of 106 lethally irradiated 6-month-old *Arsa*−/− recipients (61 with ARSA and 45 with GFP in 8 rounds of transplantation), according to a previously optimized protocol (14). To permit in situ immunodetection of ARSA, in all experiments, we used a C terminal–tagged transgene, in which the gene was fused in frame with the sequence encoding the HA peptide from the HA protein of the human influenza virus. The HA-tagged enzyme had a specific activity comparable to that of the unmodified enzyme and was properly sorted to the lysosomal compartment (21).

By measuring ARSA activity with the para-nitrocatechol sulfate (p-NC) assay in PBMCs of treated mice 6 months after transplantation, we demonstrated a complete reconstitution of enzymatic activity and ARSA overexpression with respect to WT levels (Figure 1A). Molecular analysis demonstrated efficient engraftment of transduced cells, with 80%–100% of BM CFCs positive in LV-specific PCR (not shown) and a mean of 6 ± 3 vector copies per cell (CpC), as assessed by quantitative PCR on total BM DNA (Figure 1A). These data indicate that enzyme overexpression in hematopoietic cells is associated with multiple vector integrations. We noticed that the average ARSA activity in circulating hematopoietic cells and average LV content in BM in mice in the first 4 transplantation groups were lower than those for animals in the last 4 transplantation groups. This difference could possibly be due to variations in the infectivity of the vector batch used or in the extent of myeloablation achieved. Based on this difference, we retrospectively divided all treated animals (pool) into 2 groups (A, with lower average ARSA activity, and B, with higher average ARSA activity) and investigated dose-effect relationships for all functional parameters analyzed (Figure 1A and Table 1).

Table 2

Statistical analysis of neurophysiology data

Comparison variables	Arsa⁻/⁻ (6 mo) versus WT (6 mo)	Arsa⁻/⁻ (6 mo) versus Arsa⁻/⁻ (12 mo)	Arsa⁻/⁻ (12 mo) versus WT (12 mo)	GT (12 mo) versus Arsa⁻/⁻ (6 mo)	GT (12 mo) versus Arsa⁻/⁻ (12 mo)	GT (12 mo) versus WT (12 mo)	Group A versus group B
F wave latency	< 0.002	0.30	< 0.001	< 0.001	< 0.001	0.38	0.94
MCV	< 0.001	0.09	< 0.001	< 0.001	< 0.001	0.56	0.44
s-MEP latency	0.001	0.12	< 0.001	< 0.001	< 0.001	0.91	0.063
c-MEP latency	0.006	0.014	< 0.001	< 0.001	< 0.001	0.53	0.031
CCT	0.046	0.012	< 0.001	0.019	< 0.001	0.68	0.49
CCT/F	0.045	0.006	< 0.001	0.010	< 0.001	0.27	0.86

Data obtained from neurophysiological tests were analyzed by Student's t test (2-tail distributions, 2 samples with equal variance, α = 0.05). P value for each examined variable has been reported, considering the mentioned pairs for comparison. c-MEP, cortical MEP; MCV, motor conduction velocity; s-MEP, spinal MEP.

By challenging tissue extracts with the natural ARSA substrate N-lissamine rhodaminyl–sulfatide (LRh-sulfatide), we observed enzyme overexpression in the liver of transplanted mice (Figure 1B). Supranormal ARSA activity likely reflected the extensive liver infiltration by Kupffer cells and macrophages derived from donor-transduced HSPCs, which overexpress the enzyme. Reconstitution of sulfatide metabolism was also detected in the brains of treated mice (Figure 1D) at levels corresponding to an average 10% of WT activity in the pool of treated mice (Figure 1C). As expected, whereas ARSA reconstitution was observed in the tissues of all treated mice, its average level was significantly higher in group B versus group A (Table 1).

Functional studies were performed 6 months after the transplant and before sacrifice for all treated and control mice. Neurophysiological evaluations demonstrated complete correction of the previously established defective motor conduction upon GT. Motor-evoked potentials (MEPs) showed correction to normal range of central conduction parameters (central conduction time [CCT], CCT normalized over F wave latency, and cortical MEP latency), indicating not only prevention of further deterioration that occurs with aging but also a reversal of the already established impairment (Figure 1E). Likewise, electroneurographic recordings demonstrated normalization of motor conduction velocity and F wave and spinal MEP latencies as compared with 6-month-old untreated Arsa⁻/⁻ animals (Table 2). Importantly, both group A and group B mice showed normalization of neurophysiological abnormalities.

A rotarod test showed protection of treated mice from further impairment of motor coordination and from the development of ataxia, which occurs with aging (P = 0.72, comparing the GT pool at 12 months with age-matched WT controls) (Figure 1F and Table 3). Remarkably, when considered separately, group B mice showed significantly improved latency on the rod also with respect to the 6-month-old untreated Arsa⁻/⁻ controls (Figure 1F and Table 3), indicating near complete correction of the previously established behavioral deficit.

Histopathological analysis on the CNS and PNS was performed by toluidine blue staining on semithin sections of the brain, cerebellum, dorsal root ganglia (DRG), and sciatic nerve, applying a double-blind scoring system for metachromatic deposit accumulation, neurodegeneration, and demyelination. At the time of transplantation, Arsa⁻/⁻ mice already showed signs of neuronal damage and lipid storage in the CNS and PNS (see Figures 2 and 3 and Table 1). Small lipid storage deposits were found throughout the white matter, particularly in the fimbria and corpus callosum, and in the cerebellar white matter. Cells with pathological features were detectable in the pyramidal cell layer of the cornu Ammonis, areas 2–3 (CA2–3) regions of the hippocampal cortex and in the Purkinje cell layer of the cerebellum. In the PNS, small metachromatic deposits were detectable in Schwann cell (SC) cytoplasm and in sensory neurons of DRG. By 12 months, the neuronal damage in the CNS and PNS was more severe, and the number and size of metachromatic deposits increased significantly. Furthermore, demyelination of nerve fibers in the PNS became progressively more evident, as confirmed by electron microscopy (EM) studies. Remarkably, in GT–treated mice, we observed a marked reduction of all of the neuropathological features described above (Figure 2). In the hippocampus CA2–3 and in the Purkinje cell layer of the cerebellum, the total number of neurons was higher and the fraction of neurons showing signs of degeneration (percentage over the total number of neurons) was reduced as compared with age-matched mock-treated Arsa⁻/⁻ mice (Figure 2). Interestingly, when group B mice were considered separately, the

Table 3

Statistical analysis of behavior data

Comparison	Arsa⁻/⁻ (6 mo) versus WT (6 mo)	Arsa⁻/⁻ (6 mo) versus Arsa⁻/⁻ (12 mo)	Arsa⁻/⁻ (12 mo) versus WT (12 mo)	GT (12 mo) versus Arsa⁻/⁻ (6 mo)	GT (12 mo) versus Arsa⁻/⁻ (12 mo)	GT (12 mo) versus WT (12 mo)	Group A versus group B
Two-way ANOVA	<0.001	<0.0001	<0.0001	0.104[A] <0.01[B]	<0.0001	0.72[A] 0.8[B]	<0.05

Data obtained from rotarod test were analyzed using 2-way ANOVA for repeated measurements. [A]Pool; [B]group B.
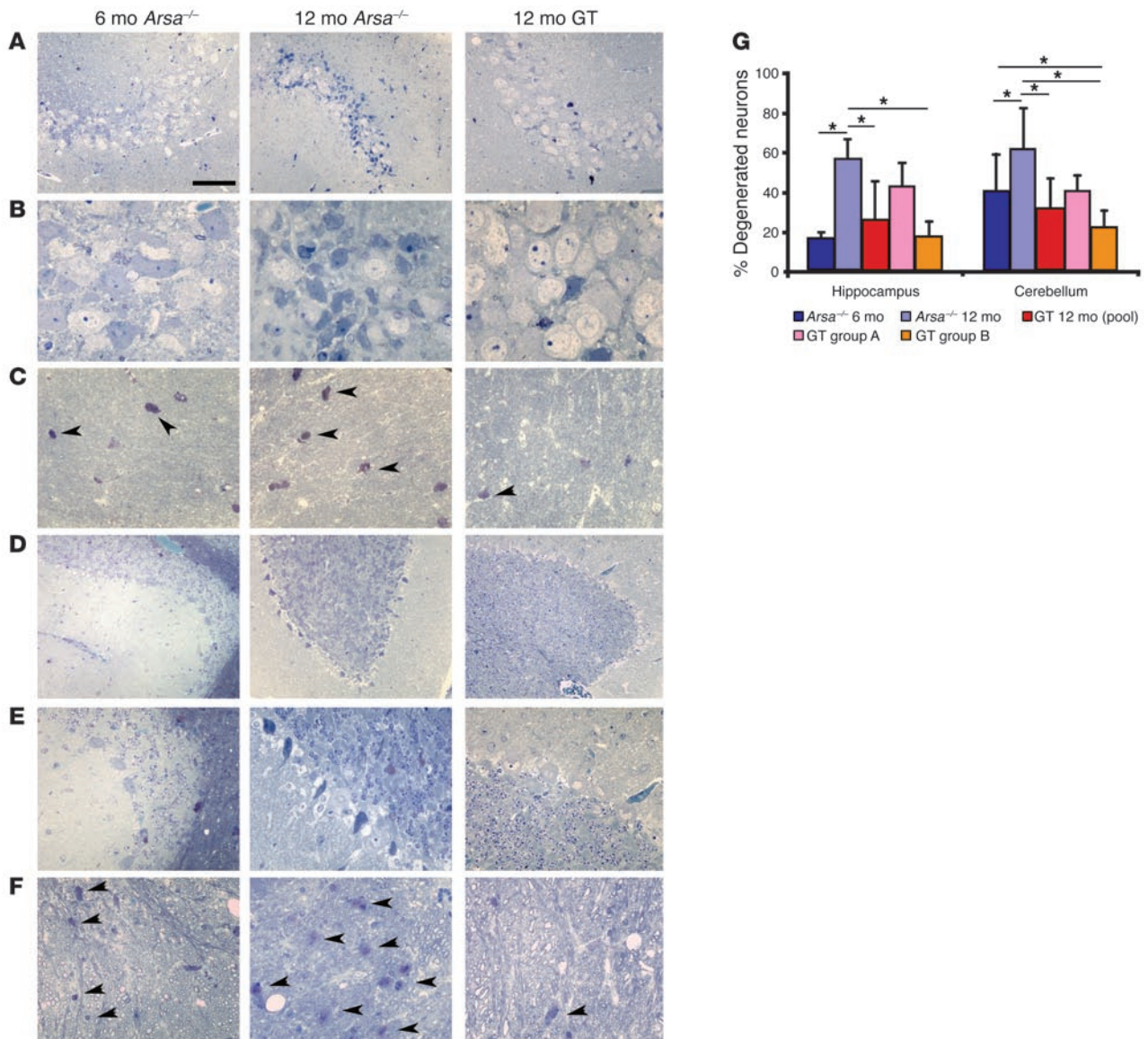
Figure 2
Correction of sulfatide storage and neuronal damage in the CNS of GT-treated mice. Transverse semithin sections of the hippocampal CA2–3 regions (**A** and **B**) and fimbria (**C**), the cerebellar Purkinje cell layer (**D** and **E**), and white matter (**F**) of untreated and mock-treated $Arsa^{-/-}$ mice (6 and 12 months old, as indicated), and 12-month-old GT mice. Cells with pathological features were already detectable in the pyramidal cell layer of the hippocampus and in the Purkinje cell layer of cerebellum at 6 months (left panels). Lipid storage (arrowheads) was detected throughout the white matter, particularly in the fimbria and cerebellum. The neuronal damage became more severe and the number and size of metachromatic deposits increased significantly in 12-month-old mice (central panels). A marked reduction of sulfatide-containing metachromatic granuli in the white matter and of neuronal damage in CA2–3 and in the Purkinje cell layer was observed in GT mice (right panels). Scale bar: 120 μm (**A** and **D**); 80 μm (**B**, **C**, and **F**); and 50 μm (**E**). (**G**) Morphometric analysis of neuronal damage, shown as percentage of total counted neurons. Neurons in the CA2–3 and in the Purkinje cell layer were protected from age-related degeneration. In 12-month-old group B treated mice, reduction of degenerating neurons as compared with that of 6-month-old untreated mice was observed, indicating neuronal rescue (*$P < 0.05$).

analysis was consistent with a rescue of Purkinje cells from the damage already observed in 6-month-old, untreated $Arsa^{-/-}$ controls (Figure 2G). Consistent with the neurophysiological studies, we observed complete protection from demyelination and marked reduction of metachromatic granuli accumulation in the sciatic nerve (Figure 3D) and clearance of neuronal damage and storage in DRG within sensory neurons, satellite cells, and SCs in treated mice (Figure 3G). Comparison of the mice in the

2 treatment groups showed a better outcome of the procedure in group B, again highlighting the critical role played by enzyme overexpression in correcting already established disease.

Mechanism of disease correction by HSPC GT: occurrence of in vivo cross-correction. Subsequently, we wanted to unravel the mechanism responsible for reconstitution of sulfatide catabolism in the brains of transplanted mice and the widespread correction of CNS pathology. The most relevant issue was to demonstrate whether
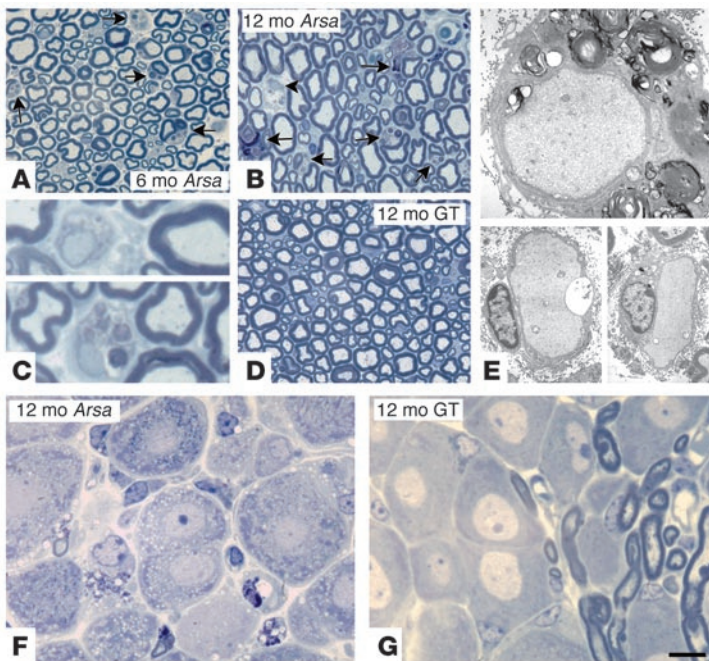
Figure 3
Correction of PNS pathology in GT-treated mice. Semithin sections and EM images from sciatic nerve and DRG are shown. (**A**) Metachromatic deposits (arrows) were detected in the SC cytoplasm of 6-month-old untreated *Arsa*⁻/⁻ mice. (**B**) By 12 months of age, the number and size of metachromatic deposits in SCs increased, and demyelination of nerve fibers became more apparent (arrowhead), as also shown at higher magnification in **C** and in detail by EM in **E**. (**D**) In GT mice, neither sulfatide storage nor demyelination was observed. (**F**) Metachromatic deposits and intracytoplasmatic vacuolation were present in sensory neurons as well as in satellite cells and SCs in DRG of 12-month-old *Arsa*⁻/⁻ mice. (**G**) In GT mice, these alterations were almost completely absent. Scale bar: 20 μm (**A**, **B**, **D**, **F**, and **G**); 5 μm (**C**); and 1.5 μm (**E**).

active enzyme was secreted by gene-corrected microglia and distributed throughout the brain of treated mice. We performed immunofluorescence studies on brain sections to detect the presence of the tagged ARSA and localize it at the cellular and subcellular levels. Confocal analysis showed widespread occurrence of tagged enzyme within both F4/80- and isolectin B4–positive microglia cells (Figure 4A) derived from donor transduced HSPCs (14, 22) and resident, neuron-specific nuclear protein–positive (NeuN-positive) neurons in diverse areas of the CNS (Figure 4, C and E). The HA-tagged enzyme was particular abundant in the cerebellum, where up to 80%–90% of calbindin-D28k–positive Purkinje cells were positive for HA staining (Figure 4E). In both microglia and neurons, the enzyme appeared to be sorted at least in part to the lysosomal compartment, as shown by colocalization of HA and lysosome-associated membrane protein 1 (Lamp1) signals (Figure 4, D and F). We and others, using intracellular marker genes such as GFP, have previously shown that transplanted HSPCs contribute almost exclusively to the microglia population of the CNS, with up to 25% of the resident microglia made by transgene-expressing cells 6 months after the transplantation, and that no exogenous marker gene expression can be detected in neurons following transplantation of transduced HSPCs (14, 22). Therefore, the present finding of HA-tagged ARSA enzyme (ARSA-HA) in neurons provides formal evidence for the occurrence of in vivo enzyme transfer. Moreover, confocal analysis allowed us to detect the presence of ARSA-HA within a large fraction of glial fibrillar acidic protein–positive (GFAP-positive) astrocytes (Figure 4G) and in rare myelin basic protein–positive (MBP-positive), CNPase-positive oligodendrocytes (Figure 4, H and I), suggesting that these other cell types could also be actively cross-corrected by enzyme-producing microglia. Interestingly, we found abundant ARSA-HA in adult neural stem cell–containing areas, such as the hippocampus and subventricular zone (Figure 5, A–C). Even though we could not detect proliferation in these areas in 12-month-old treated mice, as documented by negative Ki67 staining (not shown), it is

possible that cross-correction of neural progenitors occurred and contributed to the observed therapeutic benefit of GT. We also found widespread ARSA-HA distribution in different cell types in the PNS, including neurons in the DRG, and S100-positive SCs in the sciatic nerve of treated *Arsa*⁻/⁻ mice, proving the occurrence of enzyme transfer and cross-correction also at this critical disease site (Figure 5, D and E).

ARSA bioavailability in the CNS is exclusively dependent on recruited microglia. To investigate whether microglia cells were the effective source of enzyme in the CNS of treated mice or whether the wide distribution of ARSA was dependent on its transport from the plasma across the BBB, we generated mice bearing a stable source of ARSA-HA in the liver. We used as a liver transplant model the fumarylacetoacetate hydrolase–deficient (FAH-deficient) mouse (23). *FAH*⁻/⁻ mice die from liver failure in the neonatal period if not fed a specific diet (tyrosine free) or unless they receive pharmacological therapy [2-(2-nitro-4-trifluoromethylbenzoyl)-1,3-cyclohexanedione (NTBC), blocking tyrosine degradation]. Grompe and coworkers have shown that transplantation of WT hepatocytes effectively repopulates the mouse liver, demonstrating their strong competitive growth advantage and allowing long-term survival of the mice and complete rescue of the lethal phenotype (24). We generated transgenic mice for ARSA-HA, using the same LVs used for transplantation studies, and established a line of mice showing ARSA overexpression. These mice were viable, fertile, and without evident signs of pathology, even in the presence of high levels of ARSA expression in all tissues (data not shown). We used these mice as donors of ARSA-overexpressing, *FAH*⁺/⁺ hepatocytes to be transplanted into *FAH*⁻/⁻ mice. To avoid immune rejection, we used as recipients FAH/RAG1 double-mutant mice, which lack mature B and T lymphocytes (25). Three months after transplantation and periodic discontinuation of NTBC treatment to allow donor hepatocyte engraftment, histopathology on liver sections demonstrated massive reconstitution of the *FAH*⁻/⁻ liver by FAH⁺ ARSA-HA–transgenic hepatocytes
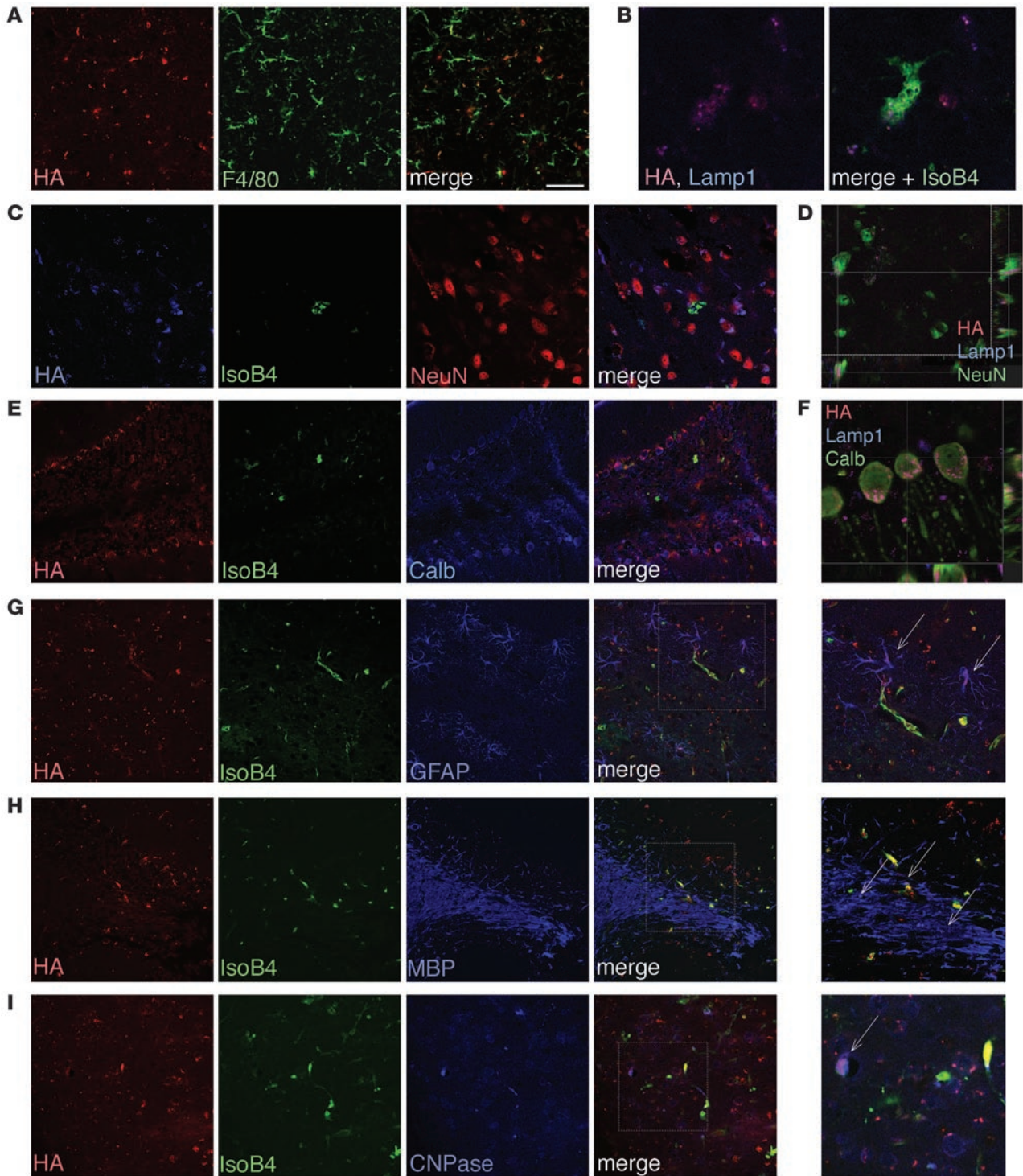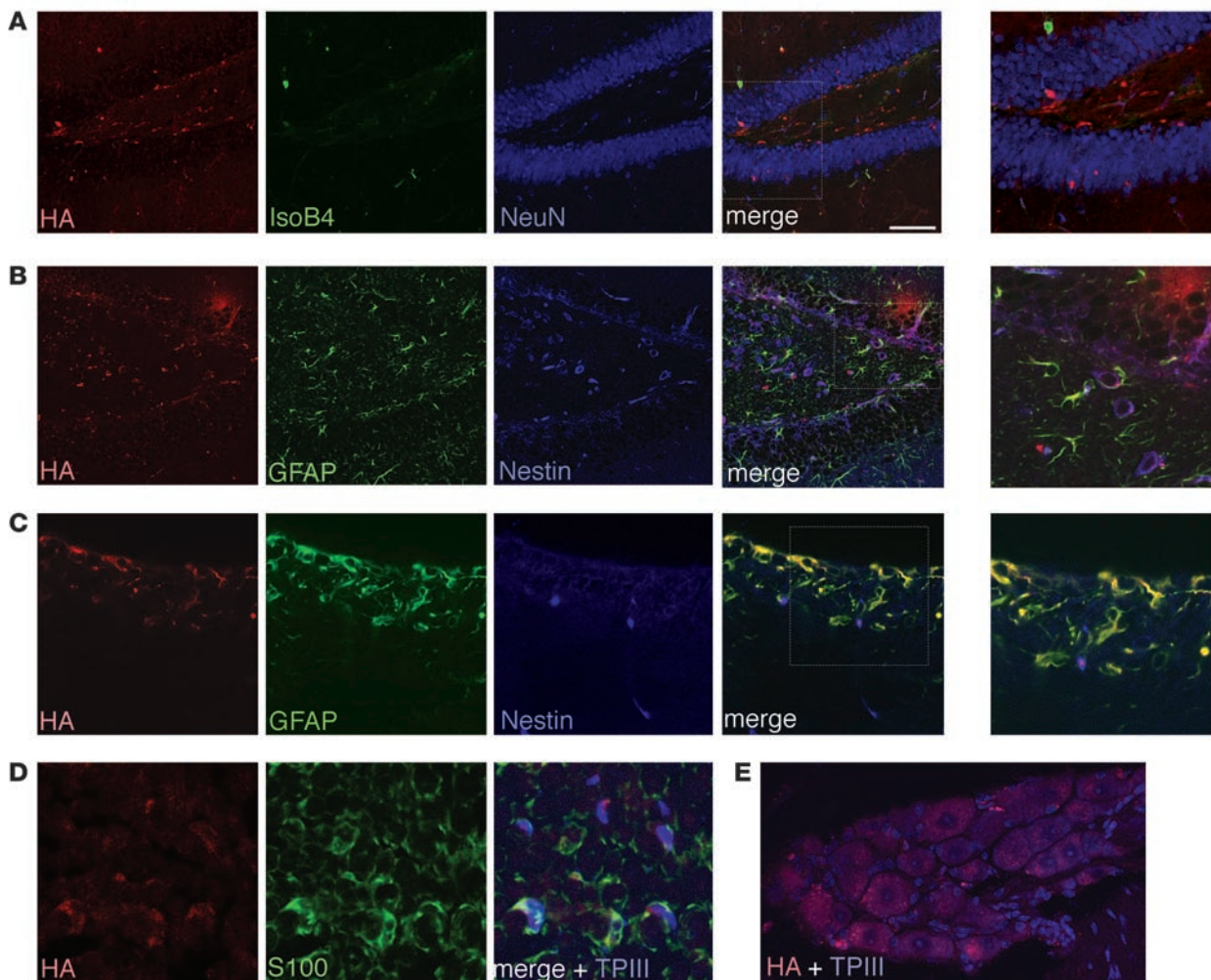
Figure 4
Enzyme biodistribution within different cell types in the nervous system of GT-treated mice. Immunofluorescence and confocal analysis of brain sections of representative mice. Single confocal planes and orthoprojections acquired in Z-stack are shown from individual and merged fluorescent signals. (**A**) HA signal was detected within microglia cells stained for the F4/80 marker. (**B**) ARSA-HA was correctly localized within the Lamp1+ lysosomal compartment of microglia, here stained for the isolectin B4 (IsoB4) marker. (**C** and **E**) HA signal was also detected within NeuN+ neurons and calbindin+ Purkinje cells (Calb) in close contact with IsoB4+ microglia, indicating the occurrence of enzyme transfer from ARSA-producing microglia to neurons. (**D** and **F**) The tagged enzyme was correctly sorted to the lysosomal compartment in NeuN+ neurons and calbindin+ Purkinje cells. (**G–I**) ARSA-HA was also detected in GFAP-positive astrocytes (**G**, magnification shown in far right panel) and in a few MBP-positive (**H**) and CNPase-positive (**I**) oligodendrocytes, as shown by arrows in magnified panels on the right. Scale bar: 90 μm (**E**, **G**, and **H**); 80 μm (**A** and **I**); 60 μm (**C** and magnified panels in **G** and **I**); 50 μm (**D**); 40 μm (magnified panel in **H**); 30 μm (**F**); and 20 μm (**B**).

Figure 5
Enzyme biodistribution in neurogenic areas of the CNS and in the PNS of GT-treated mice.Immunofluorescence and confocal analysis of brain (**A**–**C**), sciatic nerve (**D**), and DRG (**E**) sections of representative mice. Single confocal planes and orthoprojections acquired in Z-stack are shown from individual and merged fluorescent signals. (**A**–**C**) The ARSA-HA was found in adult neural stem cell areas, such as in the hippocampus (**A** and **B**), within different cell types, including NeuN, GFAP- and nestin-positive cells, and in the subventricular zone (**C**), within GFAP-positive and nestin-positive cells. (**D** and **E**) In the PNS, ARSA-HA was detected in S100-positive SCs in the sciatic nerve (**D**) as well as in sensory neurons in DRG (**E**). Scale bar: 60 μm (**A**); 50 μm (**E**); 40 μm (**B** and **C**); and 15 μm (**D**). TPIII, Topro III.

(Figure 6, A–D). Quantitative PCR for LVs performed on liver DNA confirmed high engraftment of transgenic hepatocytes (Figure 6C). Importantly, we found significant levels of ARSA-HA–specific activity in liver protein extracts and in the serum of transplanted mice, as demonstrated by an immunocapture p-NC assay selectively detecting the activity of the tagged enzyme (see Methods for details) (Figure 6E). These results indicated that we had successfully established an endogenous source of tagged enzyme, which was constantly released into the circulation up to 3 months after the transplantation. We then analyzed brain, DRG, and other organs for enzyme distribution by Western blot analysis or confocal immunofluorescence for the HA tag. As expected, HA signal was detected in the liver of both HSPC-transplanted mice and chimeric ARSA-HA/FAH mice (Figure 6B and data not shown). Immunofluorescence and Western blot analysis demonstrated the occurrence of the tagged enzyme in the kidneys of both

HSPC-transplanted mice and liver chimeras, indicating enzyme biodistribution to visceral organs both from hematopoietic and hepatic cell sources (Figure 6, F and G). Similarly, ARSA-HA signal was observed in sections of DRG of both HSPC-transplanted and hepatocyte-transplanted mice (Figure 6H), likely indicating enzyme uptake from the bloodstream in the PNS. On the contrary, whereas positive HA signal was clearly detected in confocal images and Western blots of GT-treated mice (Figure 6, I and J), both analyses failed to detect HA signal in the brain of ARSA-HA/FAH chimeras (Figure 6, I and J).

These data indicate that the BBB is an effective obstacle to ARSA biodistribution in the brain and that the enzyme detected in the CNS of HSPC-transplanted mice must originate from HSPC-derived microglia. Moreover, they demonstrate that transplanting genetically engineered HSPCs represents an effective strategy for establishing a source of a bioavailable gene product within the CNS.
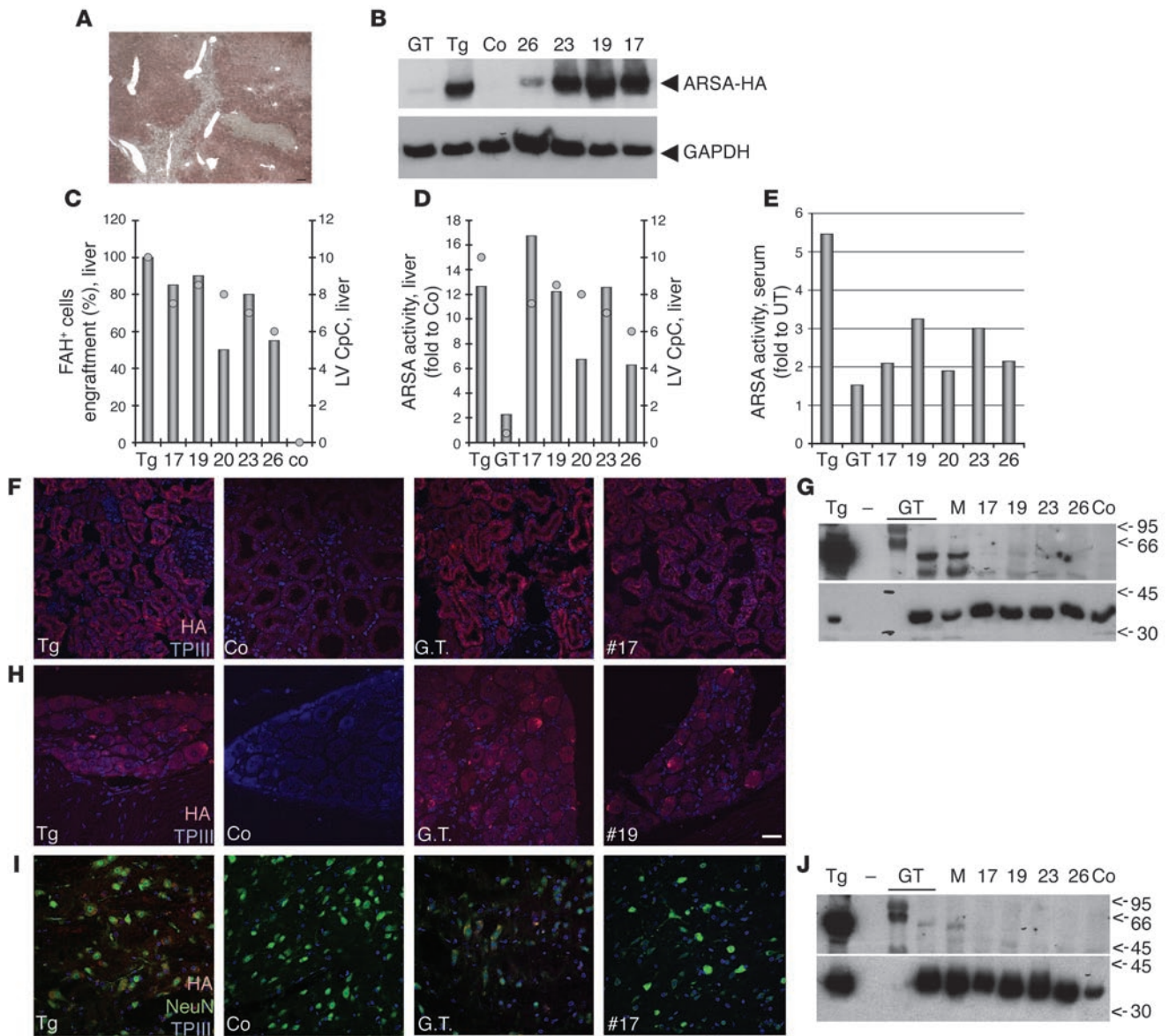
Figure 6
Enzyme biodistribution in ARSA-HA/*FAH*^{−/−} chimeras. (**A**) Immunohistochemistry of a liver section from a representative chimeric mouse showing FAH[+] hepatocytes from ARSA-HA–transgenic donors repopulating the *FAH*^{−/−} recipient. Scale bar: 20 μm. (**B**) Western blot analysis of liver samples from chimeric (nos. 17, 19, 23, and 26), control *FAH*^{+/−} (Co), GT-treated (GT: 2 different animals), and transgenic mice. Blot hybridization with anti-HA antibody (upper panel) showed ARSA-HA expression in chimeric mice and detectable protein in the GT mouse. GAPDH hybridization was used for normalization (lower panel). The engraftment of ARSA-HA, FAH[+] hepatocytes was quantified by the percentage of FAH^{+} cells on liver sections (**C**) and by ARSA-HA activity of liver samples, expressed as fold increase compared with *FAH*^{+/−} levels (**D**). LV content in the liver is expressed in CpC (right *y* axes in **C** and **D**). (**E**) ARSA-HA activity was detected in the serum of GT and chimeric mice, indicating that the tagged enzyme was secreted into the bloodstream. (**F**–**J**) Confocal immunofluorescence and Western blot analysis of kidney (**F** and **G**), DRG (**H**), and brain (**I** and **J**) from representative mice. For Western blots, anti-HA hybridization is shown in the upper panels, anti-GAPDH in the lower panels, and MW markers on the right (in kDa). ARSA-HA signal was detected in the kidney and DRG of transgenic, GT, and chimeric mice. In contrast, the signal was detected only in the brain of transgenic and GT mice, not of chimeric mice, indicating that ARSA-HA could not reach the brain from the bloodstream. Scale bar: 20 μm.

Discussion

Our previous work has demonstrated the potential of genetically modified HSPCs to target the nervous system and prevent functional and neuropathological manifestations of MLD in the mouse model when treatment begins at a presymptomatic stage. These encouraging results, however, left several issues unresolved.

With respect to the efficacy of GT, we now provide evidence that an HSPC-based approach can correct already established neurologic disease manifestations and neuronal damage when applied to symptomatic MLD mice. This is relevant because (a) the mild disease phenotype observed in the MLD mouse model, as compared with the human disease, may cause us to overestimate the therapeutic impact

of the proposed strategy if its effect is limited to the most responsive condition; (b) human patients are likely to be diagnosed when already symptomatic; (c) clinical experience in LSDs with neurological involvement indicates that HSCT can at best delay disease onset and progression if administered at a presymptomatic stage and that symptomatic treatment is ineffective (9, 26).

Because the degree of efficacy of GT on symptomatic mice was dependent on the level of reconstituted ARSA activity in hematopoietic cells and in target organs, we determined that the major advantage of GT is the possibility of expressing functional enzyme well above the normal donor's levels. Regarding the mechanisms of disease correction, we prove that gene-corrected, overexpressing microglia cells are the exclusive source of bioavailable enzyme in the brain; they widely distribute ARSA and cross-correct affected neurons and glia. The detection of ARSA in the PNS of treated mice together with the correction of functional and histopathological abnormalities underlines the relevance of this approach in targeting not only the CNS, but also the widely distributed PNS network, the involvement of which is critical to a patient's prognosis.

Correction of established neurological deficits. Neurophysiological and behavioral tests demonstrated the occurrence of CNS and PNS dysfunctions already in 6-month-old $Arsa^{-/-}$ mice. The conduction deficits in the PNS and CNS might reflect a sporadic demyelination, affecting multiple fibers along their course, thus delaying overall conduction, and/or a progressive degeneration of SCs and neurons due to intracellular sulfatide accumulation. Furthermore, $Arsa^{-/-}$ mice display abnormal motor coordination and ataxia (14, 20), which may be due to the early and extensive degeneration of Purkinje cells in the cerebellum, the massive degeneration of pyramidal neurons in the CA2–3 of the hippocampus, and PNS disease.

These neurophysiological and behavioral deficits were normalized in treated mice along with the major histopathological abnormalities. Sulfatide clearance in SCs and neurons, together with prevention of demyelination and/or stimulation of remyelination in the PNS, might account for the complete reversal of motor conduction defects and, at least in part, for the improved performance at rotarod of the treated mice. More challenging is explaining the mechanism of recovery of complex functions, such as motor coordination, that involve multiple brain areas. In the cerebellum, Purkinje cells were rescued from degeneration, possibly as a consequence of intracellular ARSA reconstitution by cross-correction and progressive sulfatide clearance. Intracellular detoxification might interrupt a degenerative cascade and reconstitute functional, normal-appearing Purkinje cells. It was recently reported that, despite the lack of evidence for adult neurogenesis in the cerebellum, neural stem or progenitor cells may reside in the postnatal cerebellum (27). Recruitment of these progenitors, which possess intrinsic regional character, in a detoxified cerebellum after GT might provide a possible explanation for the recovery in number and phenotype of Purkinje cells that we have documented here. Similar considerations apply to the rescue of pyramidal neurons in the hippocampal cortex. The presence of the tagged ARSA enzyme in adult neural stem cell areas further supports this hypothesis. Additional studies are required to establish the actual mechanisms of the unexpected neuronal rescue observed in treated mice.

In vivo evidence of ARSA biodistribution in the brain and cross-correction. We provide here a long-sought-after proof of active enzyme release from HSPC-derived microglia and the enzyme's transfer to other neural and nonneural cells in the brain. These results are even more compelling in view of previous in vitro studies that

suggested the inability of macrophages and microglia to secrete uptake-competent M6P-containing ARSA (10). Because we did not investigate the presence of M6P residues on ARSA-HA, we cannot rule out whether a mechanism other than M6P-mediated uptake could mediate enzyme transfer to neurons and other glial cells. Whatever the mechanism of enzyme transfer may be, microglia represents an efficient enzyme source for neurons and glia in the brains of affected mice. Moreover, the associated correction of neuronal damage and, most importantly, of disease manifestations, demonstrates that in vivo enzyme transfer achieved robust metabolic cross-correction of the crucial CNS cell targets of the disease. Because the phenotype of the $Arsa^{-/-}$ mouse is mild and not characterized by extensive demyelination, which is typical of the human disease, the contribution of enzyme transfer to the functional rescue of oligodendrocytes is more difficult to assess. However, the lack of signs of demyelination and the finding of ARSA-positive SCs in the PNS of treated animals indicates a likely therapeutic benefit provided to myelin-forming cells.

Interestingly, our data show that microglia represents not only an effective but also a unique source of enzyme for the CNS, even in the presence of a peripheral depot. ARSA-HA/FAH chimeras sustain secretion of enzymes in the bloodstream by the repopulated liver. However, the absence of detectable tagged ARSA in the brain indicates inefficient enzyme uptake across the BBB. Enzyme detection in the PNS, on the contrary, suggests that the blood-nerve barrier may be more permeable. These data, while validating our GT strategy for enzyme targeting to the CNS, challenge the potential efficacy of protein-based enzyme replacement strategies (11) to deliver ARSA beyond the BBB. It should be noted, however, that BBB status could be affected by disease conditions, such as multiple sclerosis, or perturbed by drug treatments or irradiation, which may temporarily allow macromolecules like ARSA to reach the brain from the circulation. However, neither in MLD patients nor in $Arsa^{-/-}$ mice has BBB leakiness been reported to date.

Safety concerns on LV gene transfer and enzyme overexpression in HSPCs. The dose-effect relationship described herein underlines the key role played by enzyme overexpression in hematopoietic cells and microglia, suggesting a requirement for high engraftment of transduced cells and supranormal levels of enzymes in these cells to achieve significant therapeutic effects on the nervous system. Extensive engraftment of transduced cells can be achieved by coupling a myeloablative conditioning regimen with an efficient transduction of HSPCs. Efficient HSPC transduction and enzyme overexpression raise safety concerns with respect to both vector integration load and the efficiency of enzyme activation.

In the context of the LVs developed for this application, high transgene expression relies on multiple vector integrations into HSPCs, a condition that increases the risk of integration-dependent genotoxicity. After the report of adverse events occurring in some GT-treated X-linked SCID patients (28), the risk of retroviral vector (RV) mutagenesis and leukemogenesis must be carefully evaluated. Both RVs and LVs have been shown to feature a bias for integration within expressed genes, thus making transcriptional interaction between the vector and flanking endogenous genes more likely (28). The advanced self-inactivating design and the moderately active internal promoter of the LVs used in our studies provide safety features that should limit such interference. In addition, several differences in lentiviral and oncoretroviral biology and pathogenesis suggest that the risk of insertional mutagenesis may be significantly lower for

LVs than for RVs (29, 30). We have been performing long-term follow-up studies of all transplanted mice in this study and, using FACS analysis and necroscopy, we never detected hematopoietic abnormalities suggestive of clonal outgrowth or underlying hematologic malignancy.

Regarding the biochemical consequences of ARSA overexpression, the identification of sulfatase-modifying factor 1 (SUMF1) as a common activator of sulfatases and a rate-limiting factor in the biological activation of these enzymes raises concerns about possible adverse effects of enzyme overexpression within certain cell types (31). In fact, overexpression of one type of sulfatase may lead to its inefficient activation and even to reduced activity of the other sulfatases by competition for their common activator. To date, we have accumulated substantial in vitro and in vivo evidence, including the study of the transgenic mice overexpressing ARSA described here, that indicates efficient enzyme activation even at supranormal expression levels, without detectable signs of cellular or organ toxicity, thus strongly alleviating these concerns (A. Biffi and M.P. Cosma et al., unpublished observations).

In conclusion, the therapeutic benefits observed in affected mice together with a detailed understanding of the mechanism of disease correction shown here strongly support clinical testing of HSPC GT in MLD patients.

Methods

Mouse studies. $Arsa^{-/-}$ MLD mice were bred in the H.S. Raffaele animal research facility by intercrossing the homozygous offspring of 2 carrier mice obtained by rederivation (embryo transfer) of $Arsa^{-/-}$ males with C57BL/6 females. Thus, the MLD mice used in this study have a mixed C57BL6/129 genetic background. WT C57BL/129 hybrid mice were purchased from The Jackson Laboratory and used as the most appropriate controls for functional studies. ARSA-HA–transgenic mice were generated as described below and bred in our animal facility. $FAH^{-/-}RAG1^{-/-}$ mice were transplanted and housed in a dedicated facility in the Department of Comparative Medicine, Oregon Health and Science University, Portland, Oregon, USA. All procedures were approved by the Institutional Animal Care and Use Committee of the Oregon Health and Science University and by the Animal Care and Use Committee of the Fondazione San Raffaele del Monte Tabor (Institutional Animal Care and Use Committee 255) and were communicated to the Ministry of Health and local authorities according to Italian law.

Neurophysiological evaluation. Mice were anesthetized with trichloroethanol, 0.02 ml/g of body weight, and placed under a heating lamp to avoid hypothermia. Neurophysiological studies were performed as described (14, 32). An unpaired Student's *t* test (2-tailed distribution, 2 samples with equal variance, α = 0.05) was performed for statistical evaluation of the data.

Rotarod. Motor learning tasks were performed with an accelerating rotarod apparatus (Ugo Basile). This rotarod equipment includes a rotating cylinder, 3.2 cm in diameter, covered with textured rubber. Each section is 6.0-cm wide, allowing 5 mice to be tested simultaneously, 1 per section. Mice walk forward on the rotating cylinder at speeds increasing from 4 to 40 rpm over a 5-minute test session. Latencies in falling off the cylinder were measured once per day for 3 days, with 3 trials per session. Statistical analyses were performed by 2-way ANOVA for repeated measurements using Scheffe's procedure as a post hoc after significant main effect of the treatment.

Histopathology and EM. Semithin and ultrathin morphological analyses were performed as described (14). Mice were anesthetized intraperitoneally with avertin and perfused with 4% paraformaldehyde (PFA) in PBS. Brain, cerebellum, DRG, and sciatic nerve were removed, postfixed in 0.12 M

phosphate buffer/2% glutaraldehyde, sectioned into 2-mm blocks, postfixed with osmium tetroxide, and embedded in epoxy resin (EPON; Miller-Stephenson Chemical Company). Semithin (1-μm-thick) sections were stained with toluidine blue. For EM, ultrathin sections were stained with uranyl acetate and lead citrate. For morphometric analysis, microscopic images were taken with a digital camera and processed by Adobe Photoshop 7.0 software. Counts were performed in double blind by 2 investigators on slides with a number-code system, and results were analyzed. Metachromatic deposits were counted in the hippocampal fimbria and cerebellar white matter; neuronal damage was evaluated in the CA2–3 of the hippocampal cortex and in the Purkinje cell layer of the cerebellum; demyelination was quantified on the sciatic nerve. Metachromatic deposits larger than 20 μm were counted at ×20 magnification; demyelinated fibers were observed at ×100 magnification and by EM. Pyramidal cell bodies in the hippocampal cortex (diameter > 20 μm) were counted between the maximal convexity of the CA3 and the transition to CA2. The normal cerebellum contains a single layer of Purkinje cells that runs throughout the cerebellum in parallel with the cortical convolutions. Purkinje cell counts were obtained for each of 10 successive parasagittal sections per mouse, using corresponding sections across mice. To be counted, a cell had to be located in the Purkinje cell layer (diameter > 20 μm). Cells with shrunken cytoplasm and irregular, darkly stained nuclei were scored as pathological. For each experimental sample, 3–6 noncontiguous sections were analyzed for $Arsa^{-/-}$ mice (n = 6 at 6 months and n = 6 at 12 months) and GT mice (n = 10), and 60–200 cells were scored per section. The average percentage of damaged neurons for each sample was considered for each experimental group for statistical analysis (Student's *t* test, 2-tail distribution, 2 samples with equal variance, α = 0.05).

LV production and titration. Vesicular stomatitis virus–pseudotyped LV stocks were produced by transient cotransfection of the transfer constructs pCCLsin.cPPT.hPGK.eGFP.Wpre or pCCLsin.cPPT.hPGK.ARSA-HA.Wpre, the third-generation packaging constructs pMD2.Lg/p and pRSV.Rev, and the pMD2.G envelope construct in 293T cells followed by ultracentrifugation of conditioned medium, as described (14). Stocks were titered by endpoint expression titer in HeLa cells and quantified for particle content by HIV-1 Gag p24 immunocapture assay.

Transduction of hematopoietic progenitors and HSCT. Six-week-old male $Arsa^{-/-}$ mice were sacrificed with CO_2, and BM was harvested by flushing the femurs and the tibias. Hematopoietic progenitors were purified using the Stem Sep Separation Kit (StemCell Technologies Inc.). For transduction, 1×10^6 cells/ml were exposed to PGK-GFP LVs (1×10^8 HeLa transducing units/ml) or PGK-ARSA-HA LVs (1–3 μg p24 equivalent/ml) in Stem-Span Serum-Free Expansion Medium (StemCell Technologies Inc.) in the absence of serum and with cytokines (100 ng/ml murine SCF, 100 ng/ml human FMS-like tyrosine kinase 3 ligand [hFlt3L], 100 ng/ml mouse IL-3, 200 ng/ml human IL-6) for 12 hours. Vector- or mock-transduced cells (10^6 cells/mouse) were injected via the tail vein into 6-month-old lethally irradiated (12 Gy in 2 administrations) $Arsa^{-/-}$ female mice.

ARSA assays. Cell pellets were lysed in 0.5 M sodium acetate, pH 5, at 4°C for 2 hours. For liver and brain samples, the tissues were homogenized in water (250 μl/100 mg of tissue), then sonicated, and centrifuged, and the supernatant was collected for ARSA activity and protein quantification. ARSA activity was detected using LRh-(12-aminododecanoyl) cerebroside 3-sulfate as substrate (LRh-CS), as described (14). ARSA activity on peripheral blood mononuclear cells was also evaluated by p-NC assay, as described (14).

PCR analyses. Clonogenic assays were performed by plating 1×10^4 BM cells in a methylcellulose-based medium (MethoCult M3434; StemCell Technologies Inc.). After 10 days, colonies were plucked and lysed for PCR analysis for the detection of LV sequences.

Genomic DNA was extracted (with an equal volume of 100 mM KCl, 10 mM Tris, pH 8.3, 2.5 mM MgCl2, and 10 mM Tris, pH 8.3, 2.5 mM MgCl2, 1% Tween-20, 1% NP-40, and proteinase K at a final concentration of 50 μg/ml) from plucked hematopoietic colonies and was subjected to PCR analysis for the PSI sequence of the LV backbone. GAPDH amplification was used to assess DNA integrity. Primers for the LV amplification were as follows: forward, 5′-TGAAAGCGAAAGGGAAACCA-3′, and reverse, 5′-CCGTGCGCGCTTCAG-3′. PCR product length was 64 bp. Primers for GAPDH amplification were as follows: forward, 5′-CGCACTTTCTTGTG-CAGTG-3′, and reverse, 5′-GTTCAGCTCTCTGGGATGAC-3′. PCR product length was 450 bp.

Vector copies per genome were quantified by TaqMan analysis starting from 200 ng of template DNA extracted from 1×10^6 total BM cell pellets, 80 mg of liver tissue, or 100 mg of brain tissue (Blood and Cell Culture DNA Midi Kit; QIAGEN). Quantitative PCR was performed by amplifying the same PSI sequence and using the same primers of the described qualitative PCR at a final concentration of 750 nmol for forward and 200 nmol for reverse primers. The probe was 5′-VIC-AGCTCTCTCGAC-GCAGGACTCGGC-MGB-3′ at a 200 nmol final concentration. As internal reference for normalization, we amplified a fragment of the murine β-actin gene using the following set of primers and probe: forward primer, 5′-AGAGGGAAATCGTGCGTGAC-3′ at 300 nmol final concentration, reverse primer, 5′-CAATAGTGATGACCTGGCCGT-3′ at 750 nmol final concentration; the probe was 5′-VIC-CACTGCCGCATCCTCTTCCTCCC-MGB-3′ at 200 nmol final concentration. A standard curve of genomic DNA carrying 5 LV copies, validated by Southern blot analysis, was constructed using DNA extracted from transgenic mouse tissue. The standard curve, based on different dilutions of DNA (from 250 to 50 ng), and accordingly, of LV copies, was used as standard both for LVs and for β-actin amplification. Reactions were carried out in a total volume of 25 μl, in an ABI Prism 7700 HT Sequence Detection System (Applied Biosystems). The number of LV CpC was calculated as follows: (ng LVs/ng endogenous DNA) × (number of LV integrations in the standard curve).

Immunofluorescence analysis. Mice were sacrificed under deep anesthesia by intracardiac perfusion with 0.9% NaCl followed by 4% PFA in PBS, pH 7.4. Organs were fixed for 10–12 hours in PFA, equilibrated for 48 hours in PBS containing 15% sucrose, and then embedded in OCT compound for quick freezing in liquid nitrogen. From 10- to 40-μm cryostatic sections were processed for immunofluorescent staining. Sections were blocked with 5% goat serum (Vector Laboratories) diluted in PBS containing 1% BSA and 0.2% Triton X-100 (PBS-T). Primary antibodies were diluted in PBS-T with 2% goat serum, 1% BSA, and 0.2% Triton X-100 as follows: IgG2aκ isotype control, clone A110-2, 1:200; F4/80 (MCAP497; Serotec), clone CI:A3-1, purified, 1:500; lectin from *Bandeiraea simplicifolia* (*Griffonia simplicifolia*) – FITCH (Sigma-Aldrich), 1:100; anti-HA high-affinity, rat monoclonal antibody (clone 3; Roche Diagnostics), 1:100; NeuN (MAB377; Chemicon International), 1:100; GFAP (MCA1909; Serotec), clone DP46.109, 1:100; MBP (MCA408; Serotec), 1:100; rabbit anti–calbindin-D28k (Swant), 1:100; mouse anti-Lamp1 monoclonal antibody (VAM-EN001; Stressgen Biotechnologies), 1:100. After incubation for 1 hour at room temperature or 12 hours at 4°C, sections were washed in PBS-T and stained for 1 hour with secondary antibodies (Alexa Fluor; Invitrogen) diluted 1:500 in PBS-T, 1% BSA. Slides were mounted with Mount-Quick Aqueous (Electron Microscopy Sciences). HA-stained sections from the brain of mice transplanted with GFP-transduced or untransduced HSPCs were used as negative controls. Confocal microscopy was performed using 3 laser confocal microscopes (Radiance 2100; Bio-Rad; Zeiss and Leica TCS SP2; Leica Microsystems). Fluorescent signals from single optical sections were sequentially acquired and analyzed by Adobe Photoshop 7.0 software.

ARSA-HA–transgenic mice generation. ARSA-HA–transgenic mice were generated using LV-ARSA-HA as described (33). Pups were genotyped for the presence of the Wpre sequence by PCR. Positive mice were bred to test germline transmission of the transgene and to generate lines of animals expressing ARSA activity in peripheral blood mononuclear cells and tissues at high (>5-fold basal levels) or medium levels (2- to 5-fold to basal levels). DNA was extracted from the tail and used to quantify vector copy number by quantitative PCR.

Hepatocytes transplantation into FAH$^{-/-}$ recipients. FAH-RAG1 double-mutant mice were generated by crossing *129S4 FAH* mutant and a *C57BL6 RAG1* mutant and subsequently used as transgenic hepatocyte recipients. All mutant mice received NTBC in their drinking water at a concentration of 16 mg/l (estimated dose of 2 mg/kg body weight) until transplantation. Hepatocytes were isolated from 2 ARSA-HA–transgenic donors with ARSA activity in peripheral blood mononuclear cells quantified as 5- to 8-fold greater than basal levels. The isolation and transplantation were performed as previously described (24, 34). Briefly, parenchymal hepatocytes were isolated by a 2-step collagenase perfusion and resuspended in 100 μl of DMEM, then 5×10^5 viable hepatocytes were injected intrasplenically. NTBC was gradually discontinued during the week after transplantation, and the weight of the transplanted animals was measured twice a week. The drug was briefly reintroduced when body weight reached 80% or less of the initial weight, but no more was administered after day 90, independently of body weight. Three months after the transplantation, following peripheral blood sampling for collection of serum, chimeric mice were sacrificed under deep anesthesia by intracardiac perfusion with 0.9% NaCl for 15 minutes to avoid interference with further analysis of ARSA-HA present in the peripheral blood. Liver, kidney, DRG, and brain were collected and processed as follows: (a) homogenized in 0.5 M Na acetate, pH 5, containing protease inhibitors and 1% SDS, for Western blot analysis; (b) fixed in 4% PFA and frozen for immunofluorescent staining; (c) stored for later DNA extraction; (d) homogenized in Na acetate for ARSA-HA–specific activity determination; and (e) fixed in formalin for FAH immunohistochemistry.

Western blot analysis. Tissues were homogenized and electrophoresed in NuPAGE polyacrylamide gels (SDS-PAGE) (Invitrogen). The nitrocellulose membranes were stained with anti-HA antibody or with mouse monoclonal antibody anti-GAPDH, incubated with chemiluminescent substrate, and then analyzed.

FAH immunohistochemistry. Liver tissue fixed in 10% phosphate-buffered formalin was dehydrated in ethanol and embedded in paraffin wax at 58°C. Four-micron sections were rehydrated and stained with a polyclonal rabbit antibody to rat FAH (kindly provided by Robert Tanguay, University of Laval, Quebec City, Quebec, Canada). The antibody was diluted in PBS and applied at a concentration of 1:300,000 at 37°C for 30 minutes. Endogenous peroxidase activity was blocked with 3% H_2O_2 and methanol. Avidin and biotin pretreatment was used to prevent endogenous staining. The secondary antibody was a biotinylated goat anti-rabbit IgG used at a dilution of 1:250 (BA-1000; Vector Laboratories). Color development was performed with the AEC detection kit (Ventana Medical Systems Inc.).

ARSA-HA–specific activity detection. A p-NC assay was adapted for ARSA-HA–specific activity detection. Elisa plates were coated with an anti-HA antibody at a concentration of 1:50 in 0.1 M NaHCO$_3$, pH 8.9, and incubated overnight at 4°C. After blocking with 10% rat serum in PBS, 100 μl of serum or tissue extracts were plated into coated wells and incubated at room temperature for 2 hours. After incubation, wells were washed 3 times with 0.05% Tween-20 in PBS, and 100 μl p-NC was then added. After 90 minutes of incubation at 37°C, p-NC was collected, the reaction was stopped by adding 1 ml/1 M NaOH to each 100 μl collected p-NC, and the final product was read at spectrophotometer (515 nm wavelength).

Statistics. Statistical analysis of the data obtained from ARSA activity measurement, CpC quantification, neurophysiological tests, and quantitative evaluation of neuronal damage and metachromatic deposits was performed using an unpaired 2-tailed Student's *t* test (2 samples with equal variance, $\alpha = 0.05$). Statistical analysis of the data obtained with rotarod test was performed using 2-way ANOVA for repeated measurements. After evidence of significant effect of the treatment, we applied Scheffe's procedure for post-hoc evaluation.

1. Aicardì, J. 1998. *Diseases of the nervous system in childhood*. Mac Keith Press. London, United Kingdom. 907 pp.
2. Lyon, G., Adams, R.D., and Kolodny, E.H. 1996. *Neurology of hereditary metabolic diseases of children*. McGraw-Hill. New York, New York, USA. 379 pp.
3. Krivit, W., Peters, C., and Shapiro, E.G. 1999. Bone marrow transplantation as effective treatment of central nervous system disease in globoid cell leukodystrophy, metachromatic leukodystrophy, adrenoleukodystrophy, mannosidosis, fucosidosis, aspartylglucosaminuria, Hurler, Maroteaux-Lamy, and Sly syndromes, and Gaucher disease type III. *Curr. Opin.Neurol.* **12**:167–176.
4. Peters, C., and Steward, C.G. 2003. Hematopoietic cell transplantation for inherited metabolic diseases: an overview of outcomes and practice guidelines. *Bone Marrow Transplant.* **31**:229–239.
5. Krivit, W., Sung, J.H., Shapiro, E.G., and Lockman, L.A. 1995. Microglia: the effector cell for reconstitution of the central nervous system following bone marrow transplantation for lysosomal and peroxisomal storage diseases. *Cell Transplant.* **4**:385–392.
6. Neufeld, E.F. 1991. Lysosomal disease. *Annu. Rev. Biochem.* **60**:257–280.
7. Neufeld, E.F., and Muenzer, J. 2001. *The metabolic and molecular bases of inherited disease*. 8th edition. McGraw-Hill. New York, New York, USA. 6338 pp.
8. Brady, R.O., and Schiffmann, R. 2004. Enzyme-replacement therapy for metabolic storage disorders. *Lancet Neurol.* **3**:752–756.
9. Escolar, M.L., et al. 2005. Transplantation of umbilical-cord blood in babies with infantile Krabbe's disease. *N. Engl. J. Med.* **352**:2069–2081.
10. Muschol, N., et al. 2002. Secretion of phosphomannosyl-deficient arylsulphatase A and cathepsin D from isolated human macrophages. *Biochem. J.* **368**:845–853.
11. Matzner, U., et al. 2005. Enzyme replacement improves nervous system pathology and function in a mouse model for metachromatic leukodystrophy. *Hum. Mol. Genet.* **14**:1139–1152.
12. Matzner, U., Harzer, K., Learish, R.D., Barranger, J.A., and Gieselmann, V. 2000. Long-term expression and transfer of arylsulfatase A into brain of arylsulfatase A-deficient mice transplanted with bone marrow expressing the arylsulfatase A cDNA from a retroviral vector. *Gene Ther.* **7**:1250–1257.
13. Matzner, U., et al. 2001. Bone marrow stem cell gene therapy of arylsulfatase A-deficient mice, using an arylsulfatase A mutant that is hypersecreted from retrovirally transduced donor-type cells. *Hum. Gene Ther.* **12**:1021–1033.
14. Biffi, A., et al. 2004. Correction of metachromatic leukodystrophy in the mouse model by transplantation of genetically modified hematopoietic stem cells. *J. Clin. Invest.* **113**:1118–1129. doi:10.1172/JCI200419205.
15. Sano, R., Tessitore, A., Ingrassia, A., and d'Azzo, A. 2005. Chemokine-induced recruitment of genetically modified bone marrow cells into the CNS of GM1-gangliosidosis mice corrects neuronal pathology. *Blood.* **106**:2259–2268.
16. Leiming, T., et al. 2002. Functional amelioration of murine galactosialidosis by genetically modified bone marrow hematopoietic progenitor cells. *Blood.* **99**:3169–3178.
17. Zheng, Y., et al. 2003. Treatment of the mouse model of mucopolysaccharidosis I with retrorally t ransduced bone marrow. *Mol. Genet. Metab.* **79**:233–244.
18. Zheng, Y., et al. 2004. Retrovirally transduced bone marrow has a therapeutic effect on brain in the mouse model of mucopolysaccharidosis IIIB. *Mol. Genet. Metab.* **82**:286–295.
19. Liu, G., Martins, I., Wemmie, J.A., Chiorini, J.A., and Davidson, B.L. 2005. Functional correction of CNS phenotypes in a lysosomal storage disease model using adeno-associated virus type 4 vectors. *J. Neurosci.* **25**:9321–9327.
20. Hess, B., et al. 1996. Phenotype of arylsulfatase A-deficient mice: relationship to human metachromatic leukodystrophy. *Proc. Natl. Acad. Sci. U. S. A.* **93**:14821–14826.
21. Luca, T., et al. 2005. Axons mediate the distribution of arylsulfatase a within the mouse hippocampus upon gene delivery. *Mol. Ther.* **12**:669–679.
22. Priller, J., et al. 2001. Targeting gene-modified hematopoietic cells to central nervous system; use of green fluorescent protein uncovers microglial engraftment. *Nat. Med.* **7**:1356–1361.
23. Grompe, M., et al. 1993. Loss of fumerylacetoacetate hydrolase is responsible for the neonatal hepatic dysfunction phenotype of lethal albino mice. *Genes Dev.* **7**:2298–2307.
24. Overturf, K., Al-Dhalimy, M., Finegold, M., and Grompe, M. 1999. The repopulation potential of hepatocyte populations differing in size and prior mitotic expansion. *Am. J. Pathol.* **155**:2135–2143.
25. Mombaerts, P., et al. 1992. RAG-1-deficient mice have no mature B and T lymphocytes. *Cell.* **68**:869–877.
26. Peters, C., and Steward, C.G. 2003. Hematopoietic cell transplantation for inherited metabolic diseases: an overview of outcomes and practice guidelines. *Bone Marrow Transplant.* **31**:229–239.
27. Klein, C., Butt, S.J., Machold, R.P., Johnson, J.E., and Fishell, G. 2005. Cerebellum- and forebrain-derived stem cells possess intrinsic regional character. *Development.* **132**:4497–4508.
28. Fischer, A., Abina, S.H., Thrasher, A., von Kalle, C., and Cavazzana-Calvo, M. 2004. LMO2 and gene therapy for severe combined immunodeficiency. *N. Engl. J. Med.* **350**:2526–2527.
29. De Palma, M., et al. 2005. Promoter trapping reveals significant differences in integration site selection between MLV and HIV vectors in primary hematopoietic cells. *Blood.* **105**:2307–2315.
30. Montini, E., et al. 2006. Hematopoietic stem cell gene transfer in a tumor-prone mouse model uncovers low genotoxicity of lentiviral vector integration. *Nat. Biotechnol.* **24**:687–696.
31. Cosma, M.P., et al. 2003. The multiple sulfatase deficiency gene encodes an essential and limiting factor for the activity of sulfatases. *Cell.* **113**:445–456.
32. Amadio, S., et al. 2005. Motor evoked potentials in a mouse model of chronic multiple sclerosis. *Muscle Nerve.* **33**:265–273.
33. Amendola, M., Venneri, M.A., Biffi, A., Vigna, E., and Naldini, L. 2004. Coordinate dual-gene transgenesis by lentiviral vectors carrying synthetic bidirectional promoters. *Nat. Biotechnol.* **23**:108–116.
34. Overturf, K., et al. 1996. Hepatocytes corrected by gene therapy are selected in vivo in a murine model of hereditary tyrosinaemia type I. *Nat. Genet.* **12**:266–273.